Available online at www.sciencedirect.com
ScienceDirect
Solid State Ionics 177 (2006) 2133–2138
SOLID STATE IONICS
www.elsevier.com/locate/ssi

A three-dimensional CFD model of direct ethanol fuel cells: Anode flow bed analysis

Ioannis Sarris [a], Panagiotis Tsiakaras [b], Shuqin Song [b], Nicholas Vlachos [a,*]

[a] *Laboratory of Fluid Mechanics and Turbomachines, Department of Mechanical and Industrial Engineering, School of Engineering, University of Thessaly-Pedion Areos, 38334 Volos, Greece*
[b] *Laboratory of Alternative Energy Conversion Systems, Department of Mechanical and Industrial Engineering, School of Engineering, University of Thessaly-Pedion Areos, 38334 Volos, Greece*

Received 1 July 2005; received in revised form 3 February 2006; accepted 3 February 2006

Abstract

This paper presents a study of the flow field and residence times in the anode flow bed of a pilot direct ethanol fuel cell (DEFC) using 3-D numerical flow modelling. The flow characteristics in the pilot DEFC anode flow bed are discussed with regard to the available data. Calculations of the flow field characteristics and residence times in a pin-type fuel cell with a modified version of an existing finite-volume computational fluid dynamics code are presented. The numerical results are in good agreement with other computational and experimental studies for the residence times and flow distribution inside the anode flow bed. The present model provides results that can be of good assistance for the improvement of specific flow bed designs.

Keywords: Direct ethanol fuel cells; Anodic flow bed; Numerical simulation

1. Introduction

The importance and the advantages of ethanol as a potential fuel for fuel cells have been already recognized worldwide. During the last years, various investigations (either experimental [1–3] or analytical and numerical [4–6]) have been dedicated to the study of the phenomena involved during the operation of a direct ethanol (or methanol) proton exchange membrane fuel cell (PEMFC). These fuels offer several advantages in comparison to hydrogen-fed PEMFCs [1], since under STP conditions they are liquids and can be processed and stored easier.

A significant amount of work has been published for hydrogen fuel cells and for direct methanol fuel cells (DMFCs). For example, several research teams investigated the methanol crossover [7] and the anode flow characteristics such as volumetric flow variation, carbon dioxide monitoring or flow bed geometry. Various flow bed designs for DMFCs have been reported, concerning simple parallel channel designs, parallel channel with multi-purpose zones, spot and mesh designs [8–10]. Arico et al. [11] recently investigated an optimal flow bed design for vapour-fed DMFCs. They found that their design has a non-negligible effect on mass transfer characteristics, consequently affecting the rate of methanol crossover. Several studies compared different compartment designs with respect to their influence on the electrochemical cell performance and the transport of carbon dioxide. Furthermore, Scott et al. [12] compared stainless steel mesh flow beds of different mesh sizes with parallel and spot designs, and showed that mesh designs may be a cost-reducing alternative. The optimal design depends on the operating conditions such as temperature and pressure of the system, which determine the state of the fluid, as well as the carbon dioxide transport. Therefore, an optimal design should be defined only according to the specific operating conditions.

Computational fluid dynamics (CFD) is a powerful technique for the study of the complex flow and transport phenomena occurring in fuel cells. Besides the low cost of numerical modelling, CFD has the additional advantage that detailed analyses of the flow field in the fuel cell can be carried

* Corresponding author. Tel.: +30 24210 74094; fax: +30 24210 74085.
E-mail address: vlachos@mie.uth.gr (N. Vlachos).

0167-2738/$ - see front matter © 2006 Elsevier B.V. All rights reserved.
doi:10.1016/j.ssi.2006.02.019

out easier for different anode compartments. A lot of research work has been done using CFD methods (finite difference, finite volume or finite element) to simulate different types of fuel cells, such as molten carbonate [13] and proton exchange membrane fuel cells [14]. Baxter et al. [15] developed a one-dimensional mathematical model for a liquid-fed direct methanol fuel cell. Kulikovsky et al. [16] studied numerically a vapour-fed direct methanol PEMFC with a 2-D model and developed a new current-collector design based on the analysis of the detailed current–density distributions in the various layers of the cell. Barreras et al. [17] investigated both experimentally and numerically the flow distribution in a PEMFC using CFD techniques and a particle image velocimetry (PIV) measurement system.

The aim of this paper is to investigate the performance of a liquid-fed pilot DEFC anode flow bed, using 3-D numerical modelling and focusing mainly on the flow field distribution and residence times in the anode compartment. This would be very helpful for the characterization and improvement of the dynamic behaviour of the fuel cell. The flow simulation was done using an existing CFD code developed further for this purpose. This code solves the Navier–Stokes flow governing equations using finite volume methods to obtain the velocity, pressure, temperature, and species concentration fields. The residence times were calculated by injecting a tracer into the anode compartment with its transport described by a time-dependent 3 D convection-diffusion equation.

To obtain an insight of the flow field, the velocity and streamline distributions within the anode compartment of the fuel cell are presented. The effect of the incoming volumetric flow rate (i.e. Reynolds number) on the calculated residence times is assessed. Results are presented of the flow field and residence times at the anodic side of the pilot DEFC bed of dimensions 2 cm × 2 cm × 2 mm shown in Fig. 1. The main goal is to assess the ability of the CFD model to predict such flow and transport phenomena by comparing with experimental data and to study the performance of the anodic bed in terms of flow and residence times for various inflow velocities.

2. Governing equations

The governing equations of the present flow are the mass, momentum, energy, and species conservation equations. The mass continuity equation for the present flow, which is assumed incompressible, is written as:

$$\nabla \cdot (\rho_{eff} \overline{V}) = S_m \tag{1}$$

where ρ_{eff} the fluid density, $\overline{V}$ the fluid velocity vector, and S_m a source term.

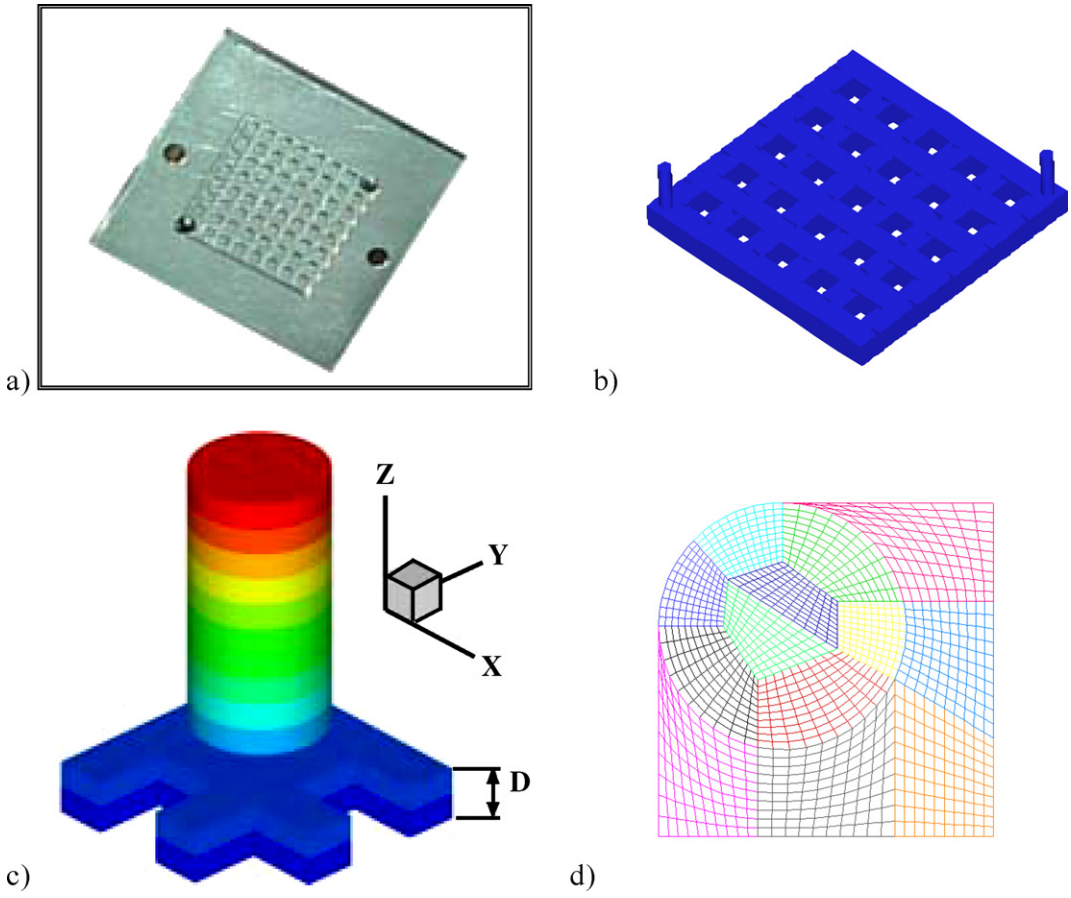

Fig. 1. Fuel cell anode flow bed geometry and discretization: (a) fuel cell anode bed, (b) computational model, (c) discretization of inlet and outlet elements, (d) connection of grid domains at the inlet element.

The source term S_m accounts for the mass balance caused by the reaction from/to the active catalytic surface. It corresponds to the consumption of ethanol and the generation of carbon dioxide on the anode. For the present simulations where the porous layers are not taken into account, S_m is considered constant and equal to the mean experimental value of ethanol consumption.

The momentum equation for the present flow, assumed time-dependent, reads:

$$\rho_{eff}\frac{\partial \overline{V}}{\partial t} + \overline{V}\cdot\nabla(\rho_{eff}\overline{V}) = -\nabla P + \nabla(\mu_{eff}\nabla\overline{V}) + S_p \quad (2)$$

where P the fluid pressure, μ_{eff} the effective fluid viscosity, and S_p a source term.

Eq. (2) is valid for both the flow duct and the porous layer (not considered here) by including a source term S_p:

$$S_p = -\left(\frac{\mu_{eff}\overline{V}}{\beta}\right) - \rho_{eff}BV_i|\overline{V}| \quad (3)$$

The first term on the right-hand side accounts for the linear relationship between the pressure gradient and the flow rate by Darcy's law, while the second is the Forchheimer term taking into account the inertial forces, the nonlinear relationship between pressure drop and flow rate [6]. This source term is zero in the flow duct, because the permeability β is infinite and, thus, Eq. (2) reduces to the regular Navier–Stokes equation. For the porous layer, the source term is nonzero, and the momentum with the nonzero source term in Eq. (3) can be regarded as a generalized Darcy model.

The energy equation reads:

$$\rho_{eff}Cp\frac{\partial T}{\partial t} + \overline{V}\cdot\nabla(\rho_{eff}C\mathrm{p}T) = \nabla(k_{eff}\nabla T) + S_T \quad (4)$$

where T, C_p and k_{eff} the temperature, specific heat and thermal conductivity of the fluid, respectively, and S_T a heat source term.

The conservation equation of a species, i, is:

$$\rho_{eff}\frac{\partial \varphi_i}{\partial t} + \overline{V}\cdot\nabla(\rho_{eff}\varphi_i) = \nabla(D_{\varphi,eff}\nabla\varphi_i) + S_{\varphi i} \quad (5)$$

where φ_i is the species mass fraction of H_2O^v, H_2O^l, CO_2, and the two phases of ethanol, $D_{\varphi,eff}$ the mass diffusion coefficient, and S_{φ_i} a mass source term corresponding to the generation/consumption of ethanol and water (vapor or liquid) during phase change.

The concentration of the inert nitrogen is determined by setting the sum of the mass fractions of all species equal to unity. It should be noted that the fluid properties in the above equations are *effective* values. For the flow duct, the effective properties are reduced to regular values of the species mixture based on composition. It has been found [6] that setting $\mu_{eff}=\mu_f$ and $\rho_{eff}=\rho_f$ (f for fuel) provides good agreement with experimental data and, thus, this approach is adopted here for simplicity.

3. Numerical procedure

The numerical method adopted is based on the solution of the unsteady Navier–Stokes equations for 3-D flows simultaneously with the energy and species conservation equations using a general structured, one-to-one matching, multi-block finite volume method. All spatial derivatives are evaluated with an accurate third-order upwind difference scheme, while a second-order Crank–Nicolson method is used for the temporal derivatives [18]. Due to the complexity of the flow geometry (Fig. 1a,b), the solution domain was divided into several blocks as shown in Fig. 1c,d. Special attention was given to the block connection of the inflow and outflow cylindrical parts with the main four-square compartment. For the range of Reynolds numbers considered in the present simulations (corresponding to laminar or creeping flow), approximately 250 blocks of a total of 2,200,000 computational cells were adequate to resolve any flow pattern and circulation.

An in-house CFD model [19–21] was appropriately modified and further developed to include variable thermo-physical properties as well as fuel and water two-phase flow calculations. The important feature of this model is based on the approach of the multicomponent two-phase mixture. The phase change and its effect on the mixture flow and heat transfer are being considered. The amount of ethanol and water during phase change are calculated from the partial pressure of ethanol or water vapour and the saturation pressure. Thus, the model is non-isothermal and non-isobaric. The present numerical model was validated against the numerical results of Perng and Street [22] and Hriberšek and Škerget [23] for the flow in a Z-shaped channel. The streamlines and the iso-vorticity lines for Reynolds number of 200 are presented in Fig. 2 and show very good agreement.

4. Results and discussion

For convenience, the numerical model uses the dimensionless form of the governing Eqs. (1)–(5) where the Reynolds number (= VD/v_{eff}) and the Peclet number (= VD/D_{e}) appear as parameters. A characteristic length equal to the width of the channel (D=1 mm) was taken, a reference concentration value of $5\times10{-}6$ mol/l, a time scale of 1 s, and a velocity of 1 mm/s. For the present simulations, the Peclet number was fixed to a value of 2×10^3, while a range of Reynolds numbers from 1 to 100 was studied. Furthermore, it was assumed that all physical properties of the mixture concerning molecular transport, especially the coefficient of mass diffusion D_{e} and the velocities are independent of concentration. These assumptions are appropriate for the present laminar flow where the very small concentrations of the added species do not alter significantly the physical properties of the background fluid. The flow simulations were carried out by starting the solution of the unsteady Navier–Stokes equations with arbitrary initial conditions and without solving the tracer concentration equation. When the flow reached steady conditions (similar to the fuel cell working conditions), the tracer was injected from the inlet and the simulations were continued until the tracer had fully reach the outlet.

4.1. Flow field distribution

Fig. 3 shows a zoom of the central region of the anode flow bed (i.e. a slice at the mid-section of the bed height ($z=D/2$) for

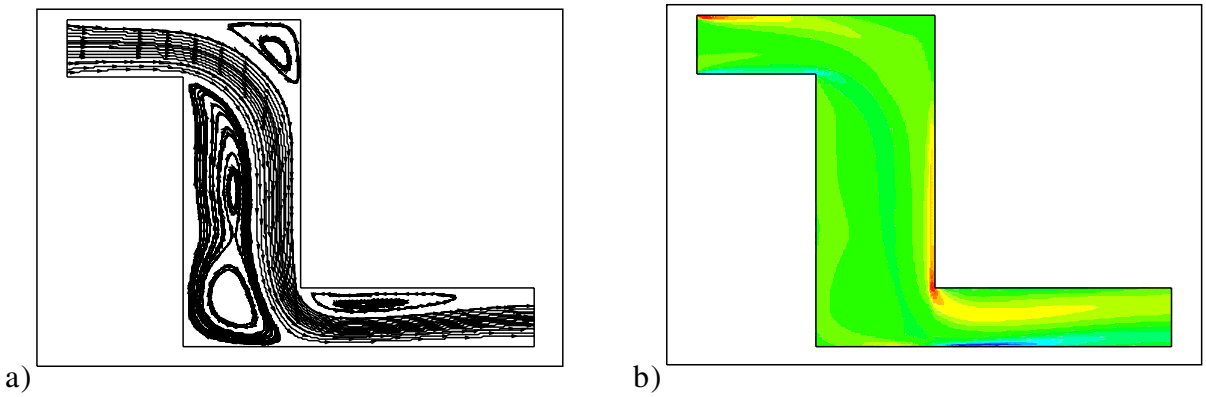

Fig. 2. Streamlines (a) and iso-vorticity lines (b) for the Z-shaped channel at $Re=200$.

convenience) showing the velocity vectors, streamlines, pressure field and the velocity magnitude distribution for Re=1. For this very low Reynolds number, no flow circulations are present and a nearly creeping flow is observed. Thus, the streamlines follow the pin-type geometry of the anode flow bed without any particular flow circulation that would be preferable for increasing the residence time. This result strongly indicates that the goal of the bed design (i.e. to enhance mixing and to increase the species residence time) is not reached for these flow conditions. The results also show that most of the fluid tends to flow from the inlet to the outlet of the channel driven through the diagonal (short) path inside the bed.

The above almost creeping flow for Re=1 is quite different from that corresponding to the higher Reynolds number case of

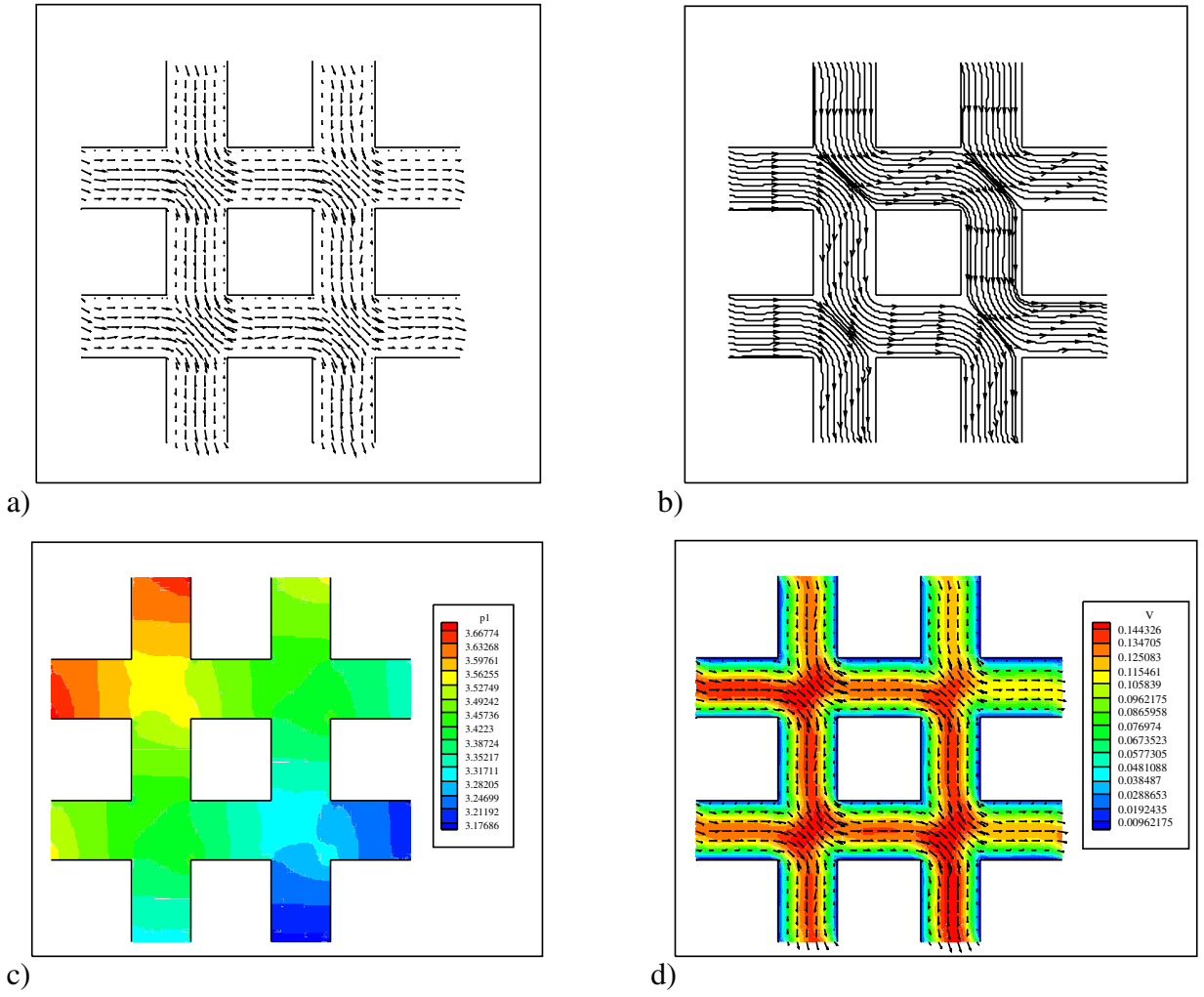

Fig. 3. Results of the anode flow bed for $Re=1$: a) velocity vectors, b) streamlines, c) pressure distribution, d) velocity magnitude at the anode flow bed mid-section.

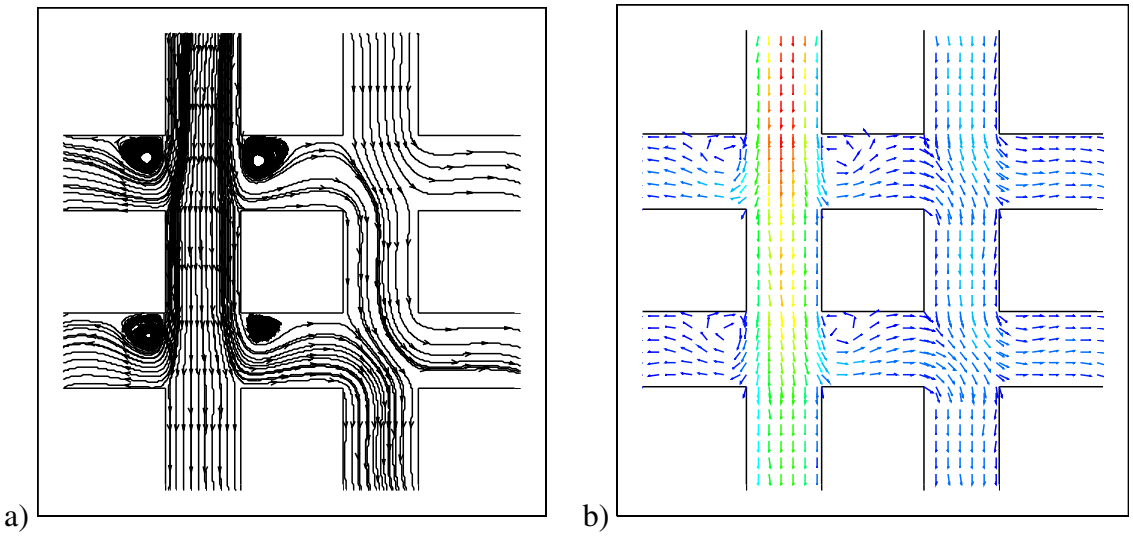

Fig. 4. Results of the anode flow bed for $Re=100$: a) streamlines, and b) velocity vectors at the upper right area of the anode flow bed (mid-section).

100, shown in Fig. 4. It must be noted that such a high Reynolds number is overoptimistic for the specific fuel cell because of the very slow reaction rates that demand slow fluid motion. However, it is a good example for assessing the design of the flow bed because it makes visible the prospective flow field (i.e. flow circulations for a specific geometry). The streamlines are used to show the position of recirculation zones, which have a large influence on the fluid distribution in the anode flow bed. It should be also noted that the recirculation bubbles, at the right side of the flow bed, are weaker than those at the left side. This means that the flow division and the pressure drop in each sub-channel result in a deceleration of the fluid. Thus, it is evident that the present anode flow bed does not satisfy the requirement of homogeneous flow distribution over the electrodes as the Reynolds number increases. The presence of particular paths of the channel along which the fluid circulates very slowly (compared to the preferred paths through the lateral channels) will probably lead to an unbalanced use of the catalyst, and a lower overall efficiency of the fuel cell.

The influence of the Reynolds number on the flow at a cross-section near the exit of the flow bed is shown in Fig. 5 where the distribution of the vertical fluid velocity is presented. For all Reynolds number studied, the flow is of Poiseuille type due to the creeping flow in each corridor of the pin-type geometry of the flow bed near the outlet. From the numerical results it appears that the velocity profiles for Re=1 and are nearly parabolic (with different magnitude because of the different inlet velocities). A significant difference is observed for Re=100, in which the vertical fluid velocity is higher than for Re=10 and, moreover, the velocity profile is no longer parabolic or symmetric.

It should be pointed out that the almost two-dimensional flow distribution observed in the present numerical simulations (away from the upper and lower walls of the anode bed) is only

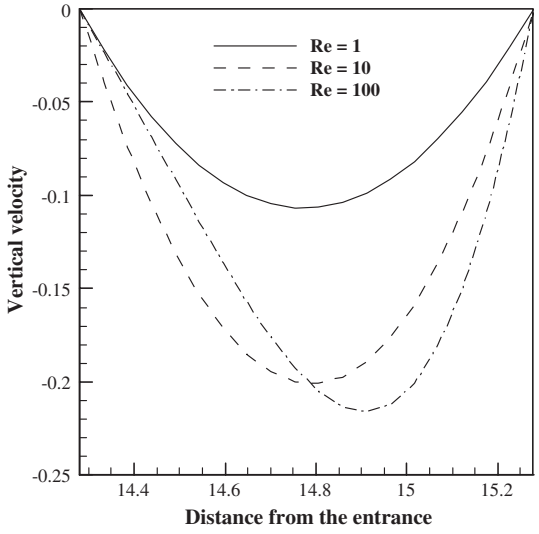

Fig. 5. Vertical velocity distribution near the exit of the flow bed for various Reynolds numbers.

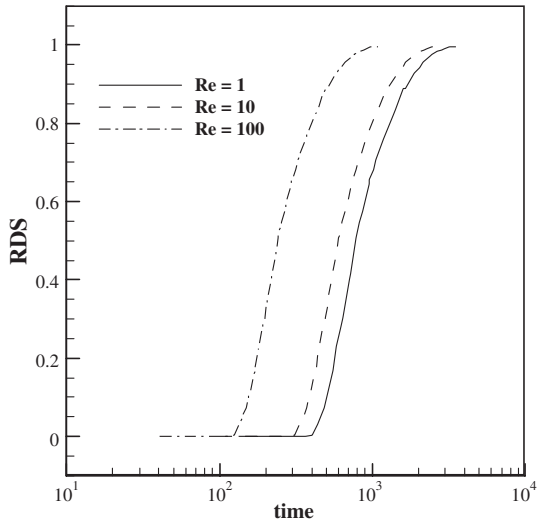

Fig. 6. Evolution of tracer concentration (RDS) at the exit indicating the residence time (non-dimensional).

representative of the particular anode flow bed geometry used. Thus, the present results cannot be extrapolated to other bed geometries. However, similar studies could be performed with alternative anode flow bed configurations, in order to calculate and assess the flow distribution in the particular cells.

4.2. Residence times

To estimate the residence time of a species in the anode flow bed, a small concentration of the species is added at the inlet pipe and its concentration at the outlet pipe is monitored during the flow calculations. For this purpose, the residence time is defined as the time elapsed for the added species concentration at the outlet pipe to reach the concentration value at the inlet pipe. This means that at the start of the simulation this ratio is zero, corresponding to the zero initial concentration of the species at the outlet. The maximum value of this ratio can be 1.0, corresponding to the situation when the concentration of the added species in the outlet pipe is the same as that in the inlet pipe. When this value is reached the simulation ends because nothing is changing in the fuel cell flow bed after that time.

The results for the residence times are summarized in Fig. 6 for the three different Reynolds numbers studied. The first conclusion that can be drawn is that the concentration of the added species in the outlet reaches its inlet value earlier when the Reynolds number increases. This indicates that the increase of the flow velocity forces the added tracer to move faster into the anode flow bed, as expected. On the other hand, the tracer remains longer in the anode flow bed for Re = 1 than for the cases Re = 10 and 100. This result indicates that the optimum bed design should be that in which the mixture velocity remains low in a flow bed compartment design that should be capable to produce circulations, thus increasing residence times, in a homogeneous way to give a balanced use of the catalyst.

5. Conclusions

The long-term objective of the present work is to develop a computational fluid dynamics (CFD) model for the study of the flow and transport phenomena in direct ethanol fuel cells. In a first attempt to assess and improve the flow performance of direct ethanol fuel cells anode compartments, calculations of the flow field were carried out. A pilot anode flow bed with inlet and outlet pipe zones was considered and the flow field and residence times were calculated. The effect of the inlet velocity (i.e. different Reynolds numbers) was found to play an important role in the bed flow and its performance optimization. Careful analysis of the velocity field and residence times of the present fuel cell anode flow bed may reveal the possible weak regions indicating the optimum solutions.

Acknowledgement

The authors are grateful to the Greek Ministry of Education for funding in the framework of the “Pythagoras 2004” program.

References

[1] S. Song, P. Tsiakaras, Appl. Catal. B Environmental (in press).
[2] W. Zhou, S. Song, G. Sun, Q. Xin, K. Poulianitis, S. Kontou, P. Tsiakaras, J. Power Sources 131 (2004) 217.
[3] S. Song, W. Zhou, Z. Liang, R. Cai, G. Sun, Q. Xin, V. Stergiopoulos, P. Tsiakaras, Appl. Catal., B Environ. 55 (2005) 65.
[4] G. Andreadis, S. Song, P. Tsiakaras, J. Power Sources (in press).
[5] G. Hu, J. Fan, S. Chen, Y. Liu, K. Cen, J. Power Sources 136 (2004) 1.
[6] J. Yuan, B. Sunden, M. Hou, H. Zhang, Numer. Heat Transf., A Appl. 46 (2004) 669.
[7] V.B. Heinzel, V.M. Barragan, J. Power Sources 84 (1) (1999) 70.
[8] W. Vielstich, A. Lamm, H.A. Gasteiger, Handbook of Fuel Cells, Fundamentals Technology and Applications, vol. 1–4, John Wiley, 2003.
[9] X. Li, I. Sabir, Int. J. Hydrogen Energy 30 (2005) 359.
[10] E. Gulzow, T. Kaz, R. Reissner, H. Sander, L. Schilling, M. Bradke, J. Power Sources 105 (2002) 261.
[11] A. Arico, P. Creti, V. Baglio, E. Modica, V. Antonucci, J. Power Sources 91 (2000) 202.
[12] K. Scott, P. Argyropoulos, P. Yiannopoulos, W. Taama, J. Appl. Electrochem. 31 (2001) 823.
[13] W. He, Q. Chen, J. Power Sources 73 (1998) 182.
[14] S. Dutta, S. Shimpalee, J.W. Van Zee, J. Appl. Electrochem. 30 (2000) 135.
[15] S. Baxter, V. Battaglia, R. White, J. Electrochem. Soc. 146 (1999) S-1-437.
[16] A. Kulikovsky, J. Divisek, A. Kornyshev, J. Electrochem. Soc 147 (3) (2000) 953.
[17] F. Barreras, A. Lozano, L. Valino, C. Marın, A. Pascau, J. Power Sources 144 (1) (2005) 54.
[18] R. Peyret. Springer-Verlag New York, 2002.
[19] I.E. Sarris, I. Lekakis, N.S. Vlachos, Int. J. Heat Mass Transfer 47 (2004) 3549.
[20] I.E. Sarris, S.C. Kakarantzas, A.P. Grecos, N.S. Vlachos, Int. J. Heat Mass Transfer 48 (2005) 3443.
[21] C.D. Dritselis, I.E. Sarris, N.S. Vlachos, 9th Conf. on Environmental Science and Technology, Rhodes, Greece, 2005.
[22] C.Y. Perng, R.L. Street, Int. J. Numer. Methods Fluids 13 (1991) 269.
[23] M. Hriberšek, L. Škerget, Comput. Methods Appl. Mech. Eng. 194 (2005) 4196.